Solar Energy Materials & Solar Cells 307 (2026) 114600

Contents lists available at ScienceDirect

Solar Energy Materials and Solar Cells

journal homepage: www.elsevier.com/locate/solmat

Unveiling the damp-heat-induced degradation mechanism of AZO-incorporated silicon heterojunction solar cells and modules

Kai Zhang [a,b,*], Muhammad Ainul Yaqin [a,b], Andreas Lambertz [a], Karsten Bittkau [a], Uwe Rau [a,b], Kaining Ding [a,**]

[a] IMD-3 Photovoltaics, Forschungszentrum Jülich GmbH, Jülich, 52425, Germany
[b] Jülich Aachen Research Alliance (JARA-Energy) and Faculty of Electrical Engineering and Information Technology, RWTH Aachen University, Aachen, 52074, Germany

ARTICLE INFO

Keywords:
Silicon heterojunction
AZO
Damp-heat-induced degradation (DHID)
Degradation mechanism

ABSTRACT

Aluminum-doped zinc oxide (AZO) film is a promising alternative to indium tin oxide (ITO), typical transparent conductive oxide (TCO) used in silicon heterojunction (SHJ) solar cells. However, the long-term damp heat (DH) stability of AZO-based SHJ devices remains a critical concern due to the moisture sensitivity of AZO. In this work, the mechanism of damp-heat-induced degradation (DHID) of AZO-incorporated SHJ solar cells and modules was systematically investigated and compared with ITO references. After 1000 h of DH exposure at 85 °C and 85% relative humidity, AZO-incorporated SHJ solar cells exhibited a larger efficiency loss than the ITO reference, mainly associated with a significant reduction in fill factor (*FF*). The *FF* degradation was strongly correlated with an increase in series resistance (R_s), and the increase in AZO film resistivity was identified as an important contributor to the R_s increase observed during DH exposure. X-ray photoelectron spectroscopy (XPS) revealed a pronounced increase in the OH^- intensity after DH testing, suggesting moisture-induced chemical modification of the AZO surface or near-surface region. Moreover, the observed open-circuit voltage (V_{oc}) degradation after DH exposure implies that moisture-related degradation may extend beyond the AZO surface and affect underlying passivation layers. In addition, scanning electron microscopy (SEM) revealed the formation of surface grooves on the AZO film after DH exposure. These observations, together with the electrical degradation of the AZO films and devices, are consistent with moisture-induced degradation of AZO. Furthermore, a MgF_2 capping layer improved the DH stability of AZO-incorporated SHJ solar cells by mitigating moisture-induced degradation.

1. Introduction

Silicon heterojunction (SHJ) solar cells have been recognized as one of the most advanced technologies for improving solar power generation [1–4]. The development of SHJ solar cells has undergone significant advancements over the past decades. LONGi has achieved 26.81% efficiency in both-side-contacted SHJ cells in November 2022 [5]. Most recently, Trinasolar reported a record-breaking power conversion efficiency of 27.08% for a 210 × 105 mm^2 bifacial SHJ solar cell in December 2024 [6]. SHJ solar cells can achieve high efficiencies owing to the high quality interface between the crystalline silicon (c-Si) wafer and the amorphous silicon (a-Si:H) layer (a-Si:H/c-Si interface), which minimizes the minority carrier recombination at the surface, resulting in a higher open-circuit voltage (V_{oc}) and fill factor (*FF*) compared to other c-Si-based technologies, such as passivated emitter rear contact (PERC) [7–10]. In addition, rear-junction SHJ bottom cells pair naturally with perovskite [11] or III-V compounds [12] top cells to form tandem devices [13,14].

Despite the numerous advantages of SHJ solar cell technology, several challenges remain. Firstly, one of the primary limitations compared to other photovoltaic concepts is the reliance on a transparent-conductive oxide (TCO) layer, typically indium tin oxide (ITO), to facilitate lateral charge carrier transport. ITO is widely used in industry due to its excellent optoelectronic properties [15], but it also introduces significant drawbacks. A major concern is the dependence on scarce and expensive elements such as indium (In), which could pose a bottleneck for largescale manufacturing and long-term sustainability of SHJ technology. To mitigate this issue, considerable research efforts

* Corresponding author. IMD-3 Photovoltaics, Forschungszentrum Jülich GmbH, 52425, Jülich, Germany.
** Corresponding author.
E-mail addresses: k.zhang@fz-juelich.de (K. Zhang), k.ding@fz-juelich.de (K. Ding).

https://doi.org/10.1016/j.solmat.2026.114600
Received 31 May 2026; Received in revised form 16 July 2026; Accepted 27 July 2026
Available online 30 July 2026

have been directed toward developing alternatives to indium-based TCOs in recent years. Promising approaches under investigation include indium-free TCOs, indium-reduced TCOs, and even TCO-free architectures [16–19]. Among these, one of the most actively explored options is replacing ITO with aluminum-doped zinc oxide (AZO) [9,20], which offers a more abundant and cost-effective solution while maintaining satisfactory electrical and optical properties. Secondly, SHJ solar cells are inherently more sensitive to moisture compared to other photovoltaic technologies, such as PERC technology. Moisture ingress, particularly under elevated temperatures, leads to damp-heat-induced degradation (DHID) in SHJ solar cells, ultimately reducing the solar module's power output over time [15,21–24]. The amorphous/crystalline interface of SHJ solar cells is susceptible to moisture, due to the oxidation of the hydrogenated amorphous silicon (a-Si:H) passivation layer. Various transparent-conductive oxides (TCOs), ITO and AZO, exhibit differing degrees of moisture resistance [20,25–29]. Moisture ingress can also affect the transparency and conductivity of TCO layers. TCO films can undergo chemical reactions with moisture, which results in a decrease in their electrical conductivity and optical transparency [30]. The AZO film has lower carrier mobility and higher resistivity [31] and is more susceptible to water vapor corrosion [32]. This results in a reported loss of conductivity [25]. AZO grows in a polycrystalline structure that favors the rapid penetration of water molecules into the crystal boundaries, which leads to the degradation of the material's electrical properties [26]. Recent studies have also revealed that environmental degradation of SHJ solar cells can be induced not only by moisture ingress but also by contaminant ions originating from solar module materials. In particular, sodium-related degradation mechanisms have been reported for SHJ devices employing conventional glass-based module architectures, where sodium migration can deteriorate TCO properties and device performance under damp heat (DH) conditions [33–36]. In contrast, the lightweight module architecture investigated in this work employs a polymer-based ethylene tetrafluoroethylene (ETFE) front sheet instead of conventional soda-lime glass. Therefore, sodium-ion contamination is not expected to be the dominant degradation pathway. Under these conditions, moisture-induced degradation of the AZO layer becomes a more critical reliability concern and is the primary focus of the present study.

In order to improve the electrical properties of AZO and to enhance the damp heat stability of the AZO film, different capping layers have been introduced and investigated in solar cells. These include aluminum oxide (Al_2O_3), silicon oxide (SiO_2), and silicon nitride (SiN_x). Adachi et al. [28] reported that a SiO_2 capping layer on the ITO layer improved the damp heat stability of SHJ solar cells. Morales-Vilches et al. [27] reported that the damp heat stability of solar cells with AZO front TCO was improved when they were capped with a SiO_2 capping layer, as this hindered the moisture-induced degradation at the AZO grain boundaries. In our previous study, we introduced a 10-nm ITO layer on top of the AZO as a capping layer. This significantly reduced the performance degradation under damp heat environmental conditions [22].

Therefore, in this study, we thoroughly investigated the changes in the optoelectronic properties and surface morphology of AZO-incorporated SHJ solar cells under damp heat environmental conditions, comparing them with ITO references. Degradation analysis was conducted on standalone TCO films, solar cells and solar modules. A strategy involving a MgF_2 capping layer was proposed to improve the DH stability of AZO-incorporated SHJ solar cells. The results of this study shed light on the degradation mechanism of AZO-incorporated SHJ solar cells and modules under damp heat environmental conditions.

2. Experiment and method

2.1. Sample preparation

2.1.1. Fabrication of SHJ solar cells

Fig. 1 illustrates the schematic structures of the SHJ solar cells incorporating different TCO layers, ITO, and AZO. For the SHJ solar cell incorporating ITO, as shown in Fig. 1(a), a 70 nm of ITO was applied as the front and rear TCO layer. For the SHJ solar cell incorporating AZO, as shown in Fig. 1(b), a 70 nm of AZO was applied as the front and rear TCO layer. These solar cells were fabricated based on our established SHJ solar cell baseline process [37]. We have previously reported on the parameter optimization of the devices with regard to the counterbalance between optical and electrical properties [31].

2.1.2. TCO sample preparation

In addition to the solar cells, TCO films on glass were also prepared. AZO and ITO films were fabricated on a Corning glass substrate using a sputtering process with a planar (1 wt% Al_2O_3/ZnO) and a tube (97/3 In_2O_3/SnO_2) target, respectively. The AZO films were deposited in radio frequency (RF) mode at a working power of 1 kW, a pressure of 1×10^{-3} mbar, and a temperature of 100 °C. Meanwhile, ITO films were prepared in direct current (DC) mode using a mixture of argon and oxygen gases, with set power, pressure and temperature of 5 kW, 3×10^{-3} mbar and 200 °C, respectively. The resulting film thickness corresponded to that required thickness for SHJ solar cells. Subsequently, to simulate the curing step in the SHJ solar cell fabrication process, the TCO film samples were annealed at 170 °C for 40 min.

2.1.3. Fabrication of solar modules

Solar modules using the above SHJ solar cells were also fabricated. Two types of solar module structure were involved: glass/glass (G/G) and front sheet/back sheet (FS/BS). All solar modules were prepared as single-cell mini-module samples measuring 210 mm × 210 mm, using M2+ (246.21 cm^2) bifacial, monocrystalline, busbar-free, n-type, rear-junction, SHJ solar cells with two types of TCO layers (ITO and AZO).

Fig. 2 shows the schematic cross-section of two different structures of single-cell mini modules: (a) a glass/glass (G/G) solar module configuration, and (b) a front sheet/back sheet (FS/BS) solar module configuration. In terms of solar module encapsulation, 3.2 mm white glass was used for the front and back covers of the glass/glass solar module. Ethylene tetrafluoroethylene (ETFE) was used for the front cover and a polyolefin-based foil with aluminum as the interlayer was used as the back sheet (hereafter referred to as Al-bs) for the lightweight front sheet/back sheet solar module. The specifications of the front sheet and back sheet are listed in Table S1 of the Supplementary Information. The

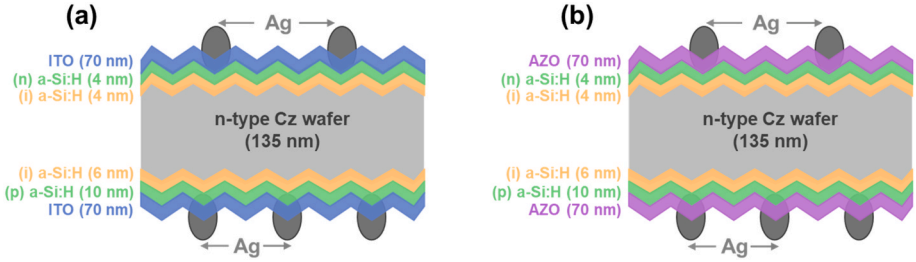

Fig. 1. Schematic cross-section of SHJ solar cells with different TCOs: (a) ITO at the front and rear sides and (b) AZO at the front and rear sides.

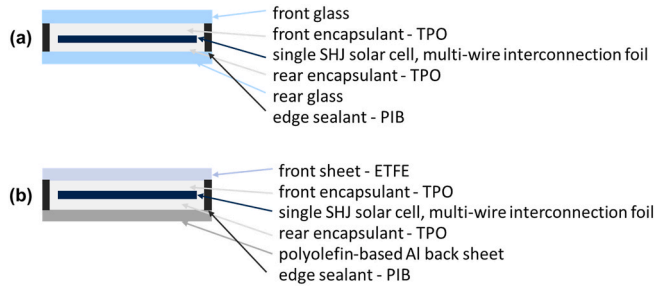

Fig. 2. Schematic of the (a) glass/glass (G/G) SHJ single-cell solar module, (b) front sheet/back sheet (FS/BS) SHJ single-cell solar module.

solar cell is embedded between the front and rear encapsulants, thermoplastic polyolefin (TPO). The specifications of the encapsulant are listed in Table S2. The solar cells were connected using multi-wire interconnection technology, which consists of 18 coated copper wires and polyethylene as the carrier foil (denoted as 'interconnection foil' or 'IF' for short). Sn-Pb-coated copper ribbons (5 mm wide and 0.2 mm thick) were used as connectors. The edges of the solar modules were sealed using polyisobutylene (PIB) tape with a width of 10 mm and a thickness of 1 mm. The specifications of the edge sealant are listed in Table S3. Table 1 summarizes the configurations of SHJ single-cell solar modules with different module structures. For each module configuration, two independent samples were prepared and tested under identical DH conditions. The parameters of the lamination process for each sample type are listed in Table S4.

2.2. Damp heat accelerated aging test

An accelerated DH aging test was conducted in a climate chamber at 85 °C and 85% relative humidity (RH) for 1000 h, in accordance with the IEC 61215 standard [38]. The current-voltage (*I-V*) characteristics and electroluminescence (EL) images of the solar cells and modules were characterized periodically at 200-h intervals during the DH test to track the aging process.

2.3. Characterization

The *I-V* characteristics [39,40] of the tested solar cell and module samples were measured using a LOANA solar cell analysis system from *PV-Tools GmbH*, equipped with Wave-Labs Sinus 220 light sources. The measurements were taken under standard test conditions (25 °C, AM 1.5G, 1000 W/m^2): (i) in the initial state, (ii) at intermediate assessment points (every 200 h of the DH test), and (iii) in the final state (after 1000 h of the DH test). The following parameters were determined: open-circuit voltage (V_{oc}), short-circuit current density (J_{sc}), series resistance (R_s), shunt/parallel resistance (R_{sh}), fill factor (*FF*), power at maximum power point (MPP) (P_{MPP}), voltage at MPP (V_{MPP}) and current at MPP (I_{MPP}).

To identify electrical homogeneity and visualize defects affecting solar cell/module performance, EL measurements were performed [41–43]. The external quantum efficiency (*EQE*) and reflectance (*R*) of the solar cells/modules were also measured using a LOANA analysis system.

Table 1
Configurations of test solar modules.

No.	Front sheet	Encapsulant (front/rear)	TCO	Interconnection	Back sheet	Quantity
1	ETFE	TPO	ITO	IF	Al-bs	2
2	ETFE	TPO	AZO	IF	Al-bs	2
3	Glass	TPO	ITO	IF	Glass	2
4	Glass	TPO	AZO	IF	Glass	2

The key electrical properties of the TCO films, such as including resistivity (ρ), carrier mobility (μ), and carrier concentration (n) were characterized by using Hall effect measurements [44,45].

3. Results and discussion

3.1. DHID of SHJ solar modules with different TCOs

Fig. 3 shows the evolution of the normalized*I-V* characteristics of the SHJ solar modules with different TCO films in different solar module configurations at fixed time intervals (200 h) during the DH test. Each value was normalized to its initial value (before the DH test). Unless otherwise stated, the results shown in the main text correspond to representative samples, while the performance evolution of all tested samples is provided in Fig. S1. After 1000 h of DH test, both ITO- and AZO-incorporated glass/glass solar modules exhibited stable performance with less than 5% relative efficiency degradation. Of these, the ITO-incorporated glass/glass solar module demonstrates superior stability, showing almost no decline in efficiency. By contrast, lightweight front sheet/back sheet solar modules display reduced stability under DH conditions compared to glass/glass modules. Notably, the AZO-incorporated front sheet/back sheet solar module experiences significant degradation, with a 52.36%$_{rel}$ reduction in efficiency after 1000 h of DH exposure. This deterioration is primarily attributed to losses in *FF*, decreased by 47.12%$_{rel}$, along with a decrease in V_{oc} and J_{sc}. The reduction in *FF* is mainly caused by a pronounced increase in R_s. It should be noted that the ITO-incorporated front sheet/back sheet solar module also exhibits some efficiency degradation after 1000 h of DH test. However, the extent of the degradation is much lower than that of the AZO-incorporated counterpart. This loss is mainly due to *FF* decreasing as R_s increase.

As can be seen from the EL images in Fig. 4, a pronounced defect appeared in the AZO-incorporated front sheet/back sheet solar module after 1000 h of the DH test. This defect is most likely due to moisture penetration leading to corrosion of the AZO films. By contrast, no such defect was found in the AZO-incorporated glass/glass solar module. This suggests that the glass/glass configuration offers better protection against moisture ingress than the front sheet/back sheet configuration. Notably, no such defects were observed in any of the ITO-incorporated solar modules, including those with a front sheet/back sheet structure. This suggests that ITO is more resistant to moisture than AZO.

Based on the above analyses, it can be concluded that AZO-incorporated SHJ solar modules are more susceptible to DHID than their ITO-incorporated counterparts. In the following section, we will therefore conduct an in-depth investigation into the degradation mechanisms affecting AZO-incorporated SHJ solar cells under damp heat conditions.

3.2. DHID of SHJ solar cells with different TCOs

3.2.1. Optoelectronic properties of SHJ solar cells

To know the DH stability of non-encapsulated SHJ solar cells, independent of the influence of encapsulants, the two bare SHJ solar cells for each TCO type were exposed to the same DH conditions as the solar modules. Fig. 5 shows the evolution of the normalized *I-V* characteristic of SHJ solar cells incorporating different TCO films, measured at fixed intervals of 200 h during the DH test. Each parameter was normalized to its initial value (before the DH test). The performance evolution for all tested samples is provided in Fig. S2. After 1000 h of the DH test, the bare AZO-incorporated SHJ solar cell exhibited a 16.38%$_{rel}$ decrease in efficiency, primarily due to a 9.84%$_{rel}$ loss in *FF*. This *FF* degradation was mainly attributed to a substantial increase in R_s. In contrast, the ITO-incorporated SHJ solar cell showed only a 2.80%$_{rel}$ reduction in efficiency over the same period.

Fig. 6 shows the evolution of EL images for SHJ solar cells with ITO and AZO TCO layers during the DH test. Pronounced EL defects were

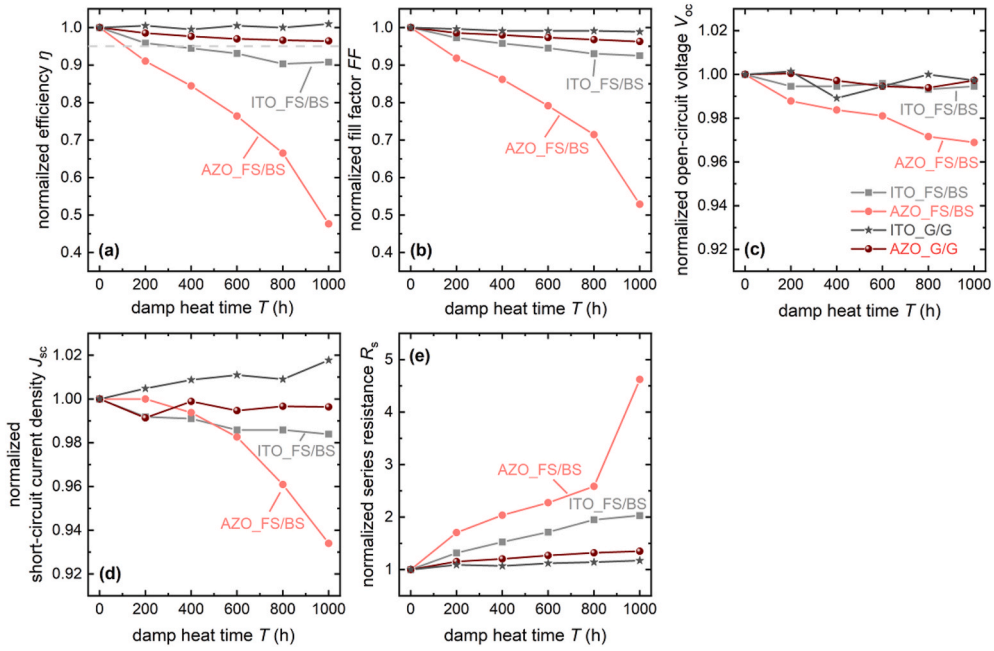

Fig. 3. Normalized values of (a) efficiency (η), (b) fill factor (*FF*), (c) open-circuit voltage (V_{oc}), (d) short-circuit current density (J_{sc}), and (e) series resistance (R_s) as a function of damp heat time for ITO-/AZO-incorporated solar modules in front sheet/back sheet (FS/BS) or glass/glass (G/G) configurations.

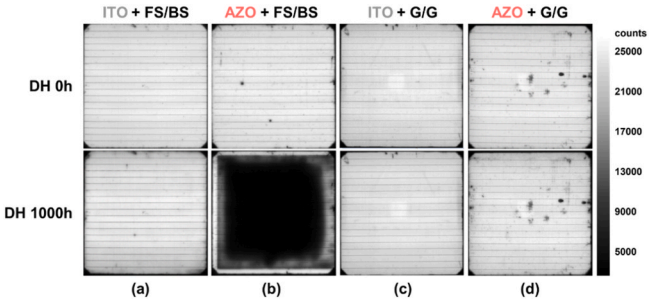

Fig. 4. EL images under low current injection ($J = 2.03$ mA/cm^2) of SHJ solar modules with ITO or AZO layer in different configurations: (a) ITO-incorporated SHJ solar module with front sheet/back sheet (FS/BS), (b) AZO-incorporated SHJ solar module with front sheet/back sheet (FS/BS), (c) ITO-incorporated SHJ solar module with glass/glass (G/G), and (d) AZO-incorporated SHJ solar module with glass/glass (G/G), taken before and after 1000 h of the DH test.

observed in the AZO-incorporated SHJ solar cell. The defect outlined in white dashed line is presumed to result from sputter-induced damage during the AZO deposition [31]. Additionally, the overall reduction in EL intensity is likely due to an increase in the resistivity of the AZO films [27]. The following section will systematically investigate the changes in the electrical properties of the standalone TCO films.

Notably, the bare AZO-incorporated SHJ solar cell exhibits less efficiency degradation and milder EL defects after 1000 h of DH exposure than the FS/BS-encapsulated AZO-incorporated SHJ solar module. As detailed in our previous study [22], the AZO layer deteriorates due to the synergistic effect of the moisture ingress and delamination of the interconnection foil in the FS/BS solar module. The delamination of the interconnection foil in AZO module can also be seen in Fig. S3. This also explains the dark rectangular shape EL defect observed in the AZO-incorporated FS/BS module after 1000 h DH exposure, as shown in Fig. 4(b). It should be noted that the degradation mechanism in the FS/BS module differs from that in the unencapsulated solar cell. While the degradation of the bare solar cell is primarily associated with moisture-induced deterioration of the AZO layer, the module degradation additionally involves interconnection foil delamination and the structure damage of AZO layer. Consequently, the AZO-incorporated FS/BS solar module exhibited even greater efficiency degradation than the unencapsulated AZO-incorporated SHJ solar cell.

3.2.2. *Electrical properties of TCO films*

In order to gain a better understanding of the performance degradation observed in SHJ solar cells under damp heat conditions, the electrical properties of standalone TCO films, specifically ITO and AZO, were investigated. Key parameters such as carrier density (n), carrier mobility (μ), and resistivity (ρ) were evaluated before and after DH exposure to assess their stability. Both types of film were deposited on Corning glass substrates using the same sputtering processes employed during solar cell fabrication. The samples were then subjected to the DH test in a climate chamber under the same conditions and for the same duration as the solar cells being tested.

Fig. 7 illustrates the evolution of key electrical parameters - carrier density, mobility, and resistivity - for both AZO and ITO films during the DH test. A significant increase in resistivity, along with a marked decrease in both charge carrier density and carrier mobility, was observed in the AZO films after 1000 h of DH exposure. Water vapor is known to be adsorbed at grain boundaries in polycrystalline AZO films can introduce trap states and increase grain-boundary potential barriers, thereby enhancing carrier scattering and reducing carrier concentration and mobility [32]. In contrast, the ITO films exhibited no notable changes in these parameters, demonstrating excellent stability and moisture resistance. These findings confirm that the combined effects of humidity and elevated temperature directly cause the dramatic rise in resistivity observed in the AZO films. This behavior is consistent with previous observations reported by Greiner et al. [25,26].

Fig. 8 illustrates the direct relationship between the series resistance of ITO- and AZO-incorporated SHJ solar cells, and the resistivity of their respective TCO films. The data clearly demonstrate that the series resistance of the AZO solar cells increases as the resistivity of the AZO films rises. Therefore, the increase in AZO film resistivity is considered an important contributor to the rise in R_s observed in AZO-incorporated SHJ solar cells during DH exposure. This correlation suggests that the degradation of the AZO layer plays a significant role in the increase in

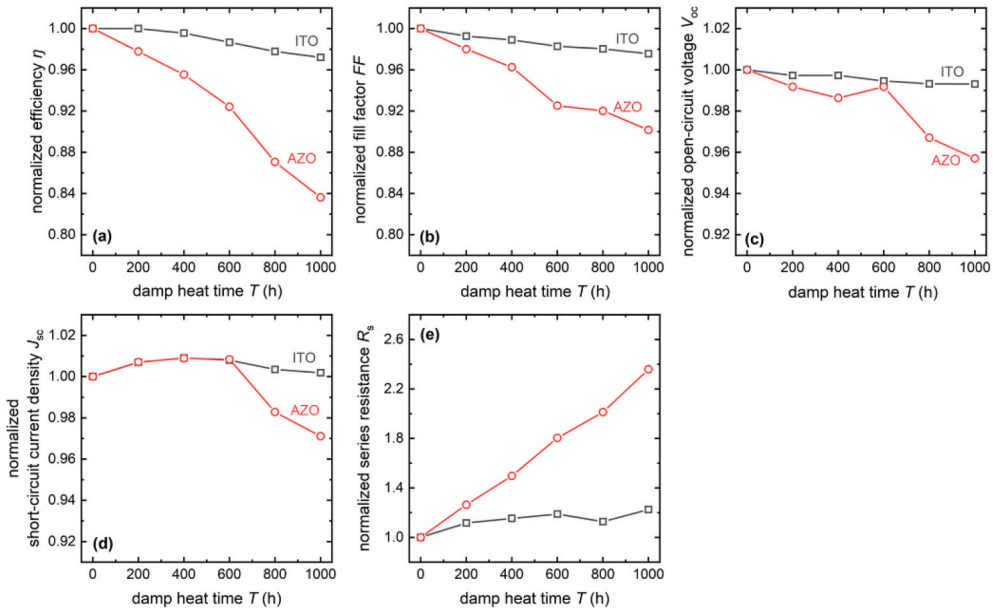

Fig. 5. Normalized values of (a) efficiency (η), (b) fill factor (*FF*), (c) open-circuit voltage (V_{oc}), (d) short-circuit current density (J_{sc}), and (e) series resistance (R_s) as a function of damp heat time for SHJ solar cells (without encapsulation) with different TCOs.

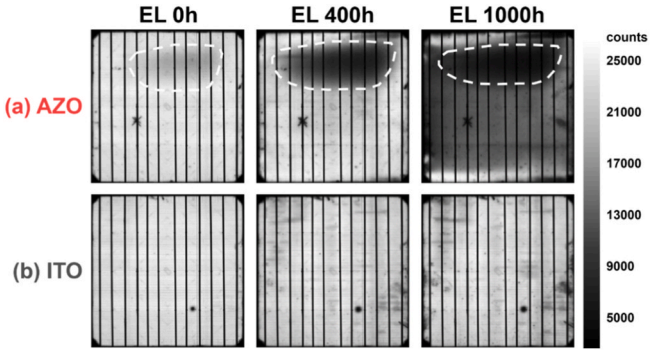

Fig. 6. EL images under high current injection ($J = 32.49$ mA/cm^2) of the SHJ solar cells with (a) AZO and (b) ITO layers taken before, after 400 h and after 1000 h of the DH test.

solar cell series resistance and the associated *FF* loss. However, other degradation pathways, including possible changes in TCO/metal contact properties and metallization-related degradation, cannot be completely excluded based on the present data. In contrast, the resistivity of the ITO film and the series resistance of the corresponding ITO solar cell only increased slightly after 1000 h of DH exposure. This confirms that the ITO film is less susceptible to damp heat corrosion.

In addition to analyzing the electrical properties, the elemental composition of AZO and ITO films was investigated using X-ray Photoelectron Spectroscopy (XPS) before and after 1000 h of the DH test. The detailed oxygen chemical states were studied by analyzing O 1s peaks of the TCOs from the XPS analysis to identify the chemisorption of the hydroxyl (OH^-) group. The peak at 530.8 eV corresponds to O^{2-} anions binding with Zn^{2+} or Al^{3+} cations. As shown in Fig. 9, the component peak at 532 eV is associated with chemisorbed O species or an OH^- group [46]. A notable increase in the intensity of the OH^- peak was observed in the AZO film after DH exposure, compared to its initial state. This suggests moisture-induced chemical modification of the AZO surface or near-surface region. In addition, the observed V_{oc} degradation after DH exposure implies that moisture-related degradation may extend beyond the AZO surface and affect underlying passivation layers. However, direct verification of moisture penetration through the entire AZO layer would require additional depth-resolved characterization. Previous studies have reported that the relatively open grain boundary structure and imperfect intergranular bonding of AZO films facilitate the diffusion of OH^- species, making the films susceptible to physical adsorption or chemical reactions [25,47]. In contrast, no significant increase in the OH^- peak intensity was observed in the ITO films, suggesting that ITO exhibits superior resistance to moisture ingress compared to AZO. $Zn(OH)_2$ formation has been proposed in previous studies as a possible degradation pathway of AZO under humid conditions, whereby zinc oxide dissolves into zinc in solution. In this case, Zn^{2+} can either be washed away with water or react with other species [48].

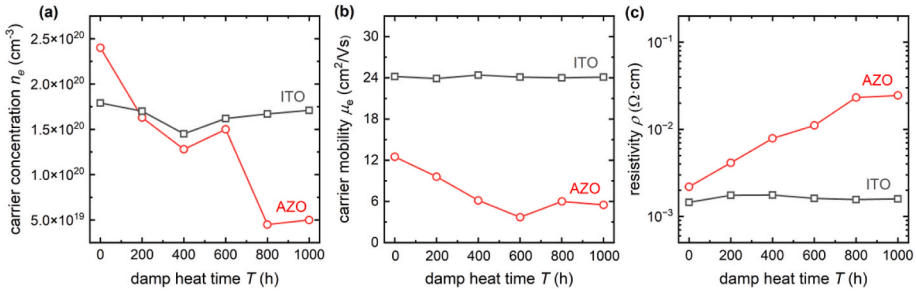

Fig. 7. Evolution of (a) carrier (electron) density (n_e), (b) carrier (electron) mobility (μ_e), and (c) resistivity (ρ) of AZO and ITO films deposited on Corning glass substrates during the DH test, measured using Hall-effect characterization.

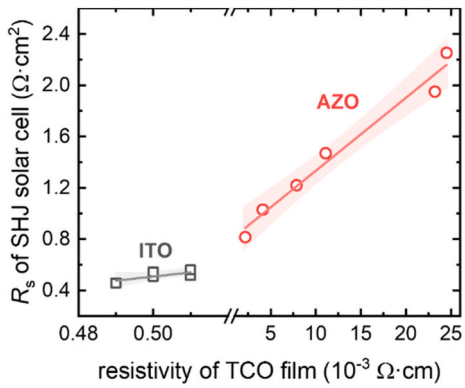

Fig. 8. Relationship between the series resistance (R_s) of ITO- and AZO-incorporated SHJ solar cells and the resistivity (ρ) of the corresponding TCO films.

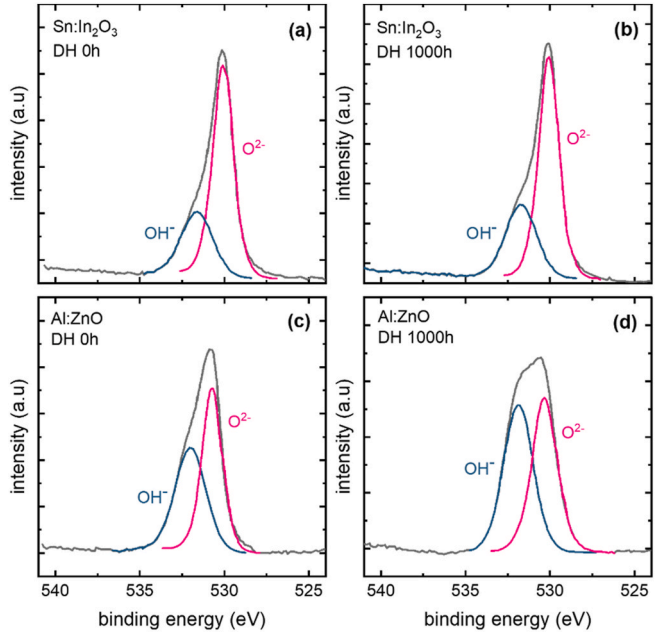

Fig. 9. XPS analysis of AZO and ITO films before and after the 1000 h of the DH test: (a) ITO before DH, (b) ITO after DH, (c) AZO before DH, and (d) AZO after DH.

It should be noted that the reversibility of the observed AZO degradation was not investigated in the present study. Post-aging annealing experiments could provide further insight into whether the degradation is dominated by reversible moisture adsorption or irreversible chemical reactions and will be considered in future work.

3.2.3. *Microstructure analysis of SHJ solar cells*

Fig. 10 shows Scanning Electron Microscope (SEM) images of AZO- and ITO-incorporated SHJ solar cells before and after 1000 h of DH test. Prior to the DH test, both the AZO and ITO films exhibited uniform and dense coverage of the textured, pyramidal silicon surface. However, after 1000 h of DH exposure, visible grooves developed on the surface of the AZO film, indicating surface corrosion. In contrast, the ITO film retained its uniform and dense structure even after prolonged exposure to DH. Previous studies have reported significant changes in the surface morphology of AZO films following DH exposure. Dhakal et al. [49] observed surface corrosion on AZO films under high-humidity conditions, with large and small spots appearing across the surface. Elemental analysis of these spots revealed the presence of contaminants such as Ca, Mg, and Si, suggesting that they may be water stains formed by moisture condensing on the sample during DH exposure. These spots can contribute to variation in resistivity. Similarly, Theelen et al. [48] found that the spots and stains consist mostly of Ca and C, but also contain O, Si and Al, while the Zn has disappeared.

The above analyses of the electrical properties, elemental composition, and surface morphology of the AZO and ITO films confirm that the AZO film is more vulnerable to moisture-induced corrosion. This makes AZO-incorporated SHJ solar cells and lightweight solar modules susceptible to degradation under damp heat conditions.

3.3. *Improve the DH stability of AZO-incorporated SHJ solar cells by MgF_2 capping layer*

In Section 3.2, we have presented the degradation of solar cells with an AZO layer during DH test. Compared with ITO reference solar cells, AZO solar cells exhibit greater efficiency degradation. In a previous study, we reported that a 10 nm ITO capping layer could be used to protect AZO and suppress the DHID of the AZO samples [22]. In this study, MgF_2 was introduced as a capping layer instead of an ITO capping layer to eliminate the use of indium completely.

Fig. 11(a) shows a schematic cross-section of AZO-incorporated SHJ solar cells with a MgF_2 capping layer. 110 nm MgF_2 layers were evaporated on front side of the solar cell after the screening-printing process. Fig. 11(b) shows the *I-V* characteristics of the AZO + MgF_2-incorporated SHJ solar cell and ITO-, AZO-references. The AZO + MgF_2-incorporated SHJ solar cell shows the highest efficiency, which is mainly attributed to the higher current resulting from the anti-reflection function of the MgF_2 layer. This can be observed in the *EQE* and reflectance curves shown in Fig. 11(c). It should be noted that the low refractive index of MgF_2 is advantageous for anti-reflection applications at air-facing interfaces. However, in encapsulated modules, where the refractive index of the encapsulant, for example ethylene-vinyl acetate (EVA), is typically higher than that of MgF_2, the anti-reflection benefit becomes much less significant. Therefore, the MgF_2 layer investigated in this work should primarily be regarded as a protective capping layer rather than an optical enhancement layer.

As shown in Fig. 11(d), the DH stability of the AZO-incorporated SHJ solar cells was significantly improved by adding a MgF_2 capping layer. The efficiency degraded by only $7\%_{rel}$ after 1000 h of the DH test, with the losses in *FF* attributed to the increase in R_s, as discussed earlier. This is a significant reduction in efficiency degradation compared with AZO SHJ solar cells without MgF_2. As can be seen from the EL images in Fig. 11(e), the EL defects after 1000 h of the DH test were significantly reduced compared to AZO solar cells without a capping layer, as shown in Fig. 6(a). This suggests that MgF_2 could be used as an effective capping layer to slow down the process of moisture penetration, thereby mitigating the moisture corrosion of the AZO layer. It should be noted that the MgF_2 layer does not act as a completely impermeable moisture barrier. Although the degradation of AZO-incorporated SHJ solar cells was significantly reduced after applying the MgF_2 capping layer, the DH stability remained inferior to that of the ITO reference cells, which maintaining 97% in initial efficiency after 1000 h of the DH test. This indicates that moisture ingress was mitigated rather than fully suppressed. Therefore, MgF_2 should be regarded as a moisture-diffusion retardant rather than a complete moisture barrier.

In the present study, the 110 nm MgF_2 layer was deposited over the entire front surface of the solar cell after screen printing, without masking the metallized regions. MgF_2-coated cells were successfully interconnected and assembled into mini-modules, and no obvious increase in the initial series resistance or reduction in efficiency was observed compared with the AZO reference devices, as shown in Table S5. However, the influence of the MgF_2 coating on solderability, contact resistance, adhesion strength, and long-term interconnection reliability has not yet been systematically investigated. These aspects will be addressed in future module-level studies.

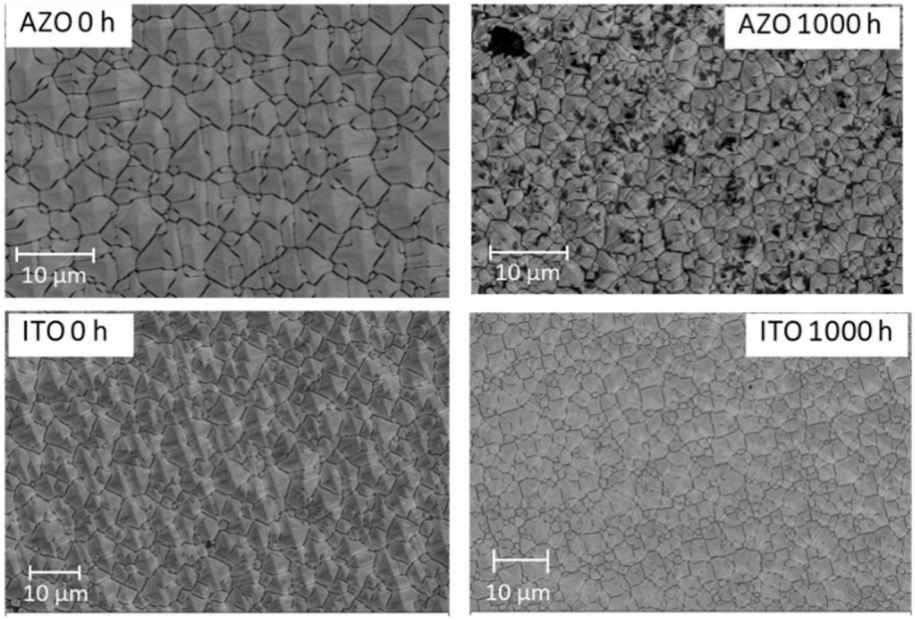

Fig. 10. SEM images of AZO- and ITO-incorporated SHJ solar cells before and after 1000 h of the DH test.

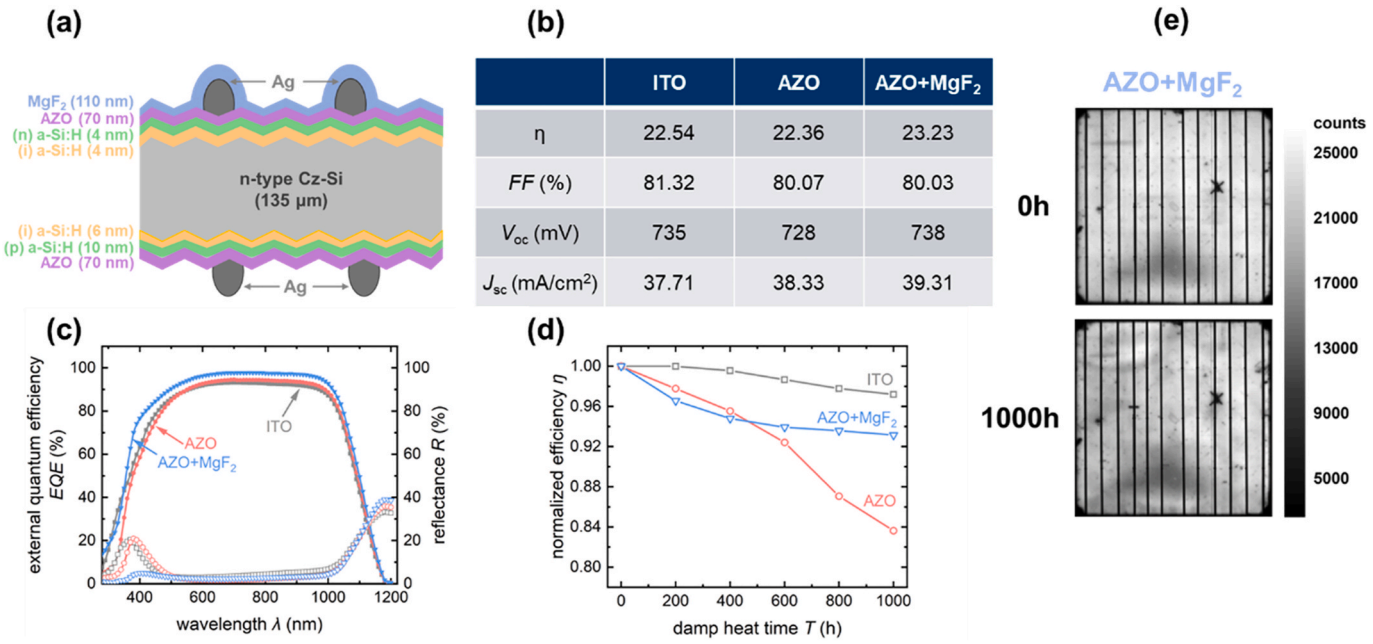

	ITO	AZO	AZO+MgF_2
η	22.54	22.36	23.23
FF (%)	81.32	80.07	80.03
V_{oc} (mV)	735	728	738
J_{sc} (mA/cm^2)	37.71	38.33	39.31

Fig. 11. (a) Schematic cross-section of AZO-incorporated SHJ solar cells with MgF_2 capping layer, (b) *I-V* characteristic parameters of SHJ solar cells incorporating different TCOs, (c) external quantum efficiency (*EQE*) and reflectance (*R*) of SHJ solar cells incorporating different TCOs, (d) normalized efficiency (η) as a function of damp heat time for SHJ solar cells with different TCO layers, and (e) EL images under high current injection ($J = 32.49$ mA/cm^2) of the AZO-incorporated SHJ solar cells with MgF_2 capping layer taken before and after 1000 h of the DH test.

It should also be noted that an ITO/MgF_2 reference structure was not included in this study. Since the primary degradation mechanism identified here is associated with the moisture sensitivity of AZO, the protective effect of MgF_2 was evaluated specifically for AZO-based SHJ devices. A systematic comparison between AZO/MgF_2 and ITO/MgF_2 structures would be valuable for determining whether the capping-layer effect is TCO-dependent and will be investigated in future work.

4. Conclusion

In this study, we thoroughly investigated the DHID mechanism in SHJ solar cells and modules with AZO films, comparing their DH stability with that of the ITO reference. The efficiency of the bare AZO-incorporated SHJ solar cell decreased by 16.38%$_{rel}$, primarily due to a 9.84%$_{rel}$ loss in *FF* after 1000 h of DH test. The *FF* degradation was strongly correlated with an increase in R_s, and the increase in AZO film resistivity was identified as an important contributor to the R_s increase observed during DH exposure. In contrast, the ITO-incorporated SHJ solar cell showed a much smaller reduction in efficiency of only a 2.80%$_{rel}$ over the same period. XPS revealed a pronounced increase in the OH^- intensity after DH testing, suggesting moisture-induced chemical modification of the AZO surface or near-surface region. Moreover,

the observed V_{oc} degradation after DH exposure implies that moisture-related degradation may extend beyond the AZO surface and affect underlying passivation layers. SEM analysis revealed visible grooves on the surface of the AZO film after 1000 h of DH exposure, indicating surface corrosion. Therefore, it is confirmed that the AZO film is more vulnerable to moisture-induced corrosion than the ITO film. This susceptibility leads to the degradation of AZO-incorporated SHJ solar cells and lightweight solar modules under damp heat conditions. It is worth noting that the degradation mechanism of the lightweight module is distinct from that of the unencapsulated solar cell. In the bare solar cell, degradation is predominantly caused by moisture-induced deterioration of the AZO layer. In contrast, module degradation additionally involves interconnection foil delamination and the structure damage of AZO layer. A MgF_2 capping layer strategy was accordingly proposed to improve the DH stability of AZO-incorporated SHJ solar cells by mitigating moisture-induced degradation. This comprehensive investigation provides substantial insight into the degradation mechanism of AZO-incorporated SHJ solar cells and modules under damp heat conditions, offering practical strategies to improve their durability and performance.

CRediT authorship contribution statement

Kai Zhang: Conceptualization, Data curation, Formal analysis, Investigation, Methodology, Validation, Visualization, Writing – original draft, Writing – review & editing. **Muhammad Ainul Yaqin:** Conceptualization, Data curation, Formal analysis, Investigation, Methodology, Validation, Visualization, Writing – review & editing. **Andreas Lambertz:** Funding acquisition, Project administration, Resources, Supervision, Writing – review & editing. **Karsten Bittkau:** Validation, Writing – review & editing. **Uwe Rau:** Supervision, Writing – review & editing. **Kaining Ding:** Funding acquisition, Project administration, Resources, Writing – review & editing.

Declaration of competing interest

The authors declare that they have no known competing financial interests or personal relationships that could have appeared to influence the work reported in this paper.

Acknowledgement

The authors would like to thank Thomas Birrenbach, Christoph Zahren, Niklas Bongartz, Volker Lauterbach, Silke Lynen, Hilde Siekmann, and Alain Doumit for their technical assistance. This work was supported by the Light.P.Roof project, which was funded by the Federal State North Rhine-Westphalia within the program “EFRE/JTF-Program NRW 2021-2027” under the grant number EFRE-20400082. Kai Zhang is grateful for the financial support from China Scholarship Council (No. 202108440128).

Appendix A. Supplementary data

Supplementary data to this article can be found online at https://doi.org/10.1016/j.solmat.2026.114600.

Data availability

Data will be made available on request.

References

[1] S.D.W. Christophe Ballif, Antoine Descoeudres, Zachary C. Holman, Semiconductors and Semimetals, Elsevier, 2014.
[2] S. De Wolf, A. Descoeudres, Z.C. Holman, C. Ballif, High-efficiency silicon heterojunction solar cells: a review, Greenpeace 2 (2012) 7–24.
[3] A. Louwen, W. van Sark, R. Schropp, A. Faaij, A cost roadmap for silicon heterojunction solar cells, Sol. Energy Mater. Sol. Cell. 147 (2016) 295–314.
[4] J. Haschke, O. Dupré, M. Boccard, C. Ballif, Silicon heterojunction solar cells: recent technological development and practical aspects - from lab to industry, Sol. Energy Mater. Sol. Cell. 187 (2018) 140–153.
[5] H. Lin, M. Yang, X. Ru, G. Wang, S. Yin, F. Peng, et al., Silicon heterojunction solar cells with up to 26.81% efficiency achieved by electrically optimized nanocrystalline-silicon hole contact layers, Nat. Energy 8 (2023) 789–799.
[6] Trinasolar, Trinasolar sets new n-type solar cell efficiency world record of 27.08. https://static.trinasolar.com/en-apac/resources/newsroom/aptrinasolar-sets-new-n-type-solar-cell-efficiency-world-record-27082024.
[7] H. Wu, F. Ye, M. Yang, F. Luo, X. Tang, Q. Tang, et al., Silicon heterojunction back-contact solar cells by laser patterning, Nature 635 (2024) 604–609.
[8] C. Ballif, F.-J. Haug, M. Boccard, P.J. Verlinden, G. Hahn, Status and perspectives of crystalline silicon photovoltaics in research and industry, Nat. Rev. Mater. 7 (2022) 597–616.
[9] B. Liang, X. Chen, X. Wang, H. Yuan, A. Sun, Z. Wang, et al., Progress in crystalline silicon heterojunction solar cells, J. Mater. Chem. A 13 (2025) 2441–2477.
[10] J.-F. Chen, H.-Z. Ren, F.-H. Hou, Z.-X. Zhou, Q.-S. Ren, D.-K. Zhang, et al., Passivation optimization and performance improvement of planar a-Si:H/c-Si heterojunction cells in perovskite/silicon tandem solar cells, Acta Phys. Sin. 68 (2019).
[11] E. Aydin, T.G. Allen, M. De Bastiani, A. Razzaq, L. Xu, E. Ugur, et al., Pathways toward commercial perovskite/silicon tandem photovoltaics, Science 383 (2024) eadh3849.
[12] K.T. VanSant, A.C. Tamboli, E.L. Warren, III-V-on-Si tandem solar cells, Joule 5 (2021) 514–518.
[13] M. He, M. Zhang, Z. Li, X. Liu, K. Sun, Z. Liu, X. Hao, Top cells for silicon-based tandem photovoltaics, Adv. Mater. 37 (2025) e2411858.
[14] O.M. Saif, A.H. Zekry, M. Abouelatta, A. Shaker, A comprehensive review of Tandem solar cells integrated on silicon substrate: III/V vs perovskite, Silicon 15 (2023) 6329–6347.
[15] O. Arriaga Arruti, A. Virtuani, C. Ballif, Long-term performance and reliability of silicon heterojunction solar modules, Prog. Photovoltaics Res. Appl. 31 (2023) 664–677.
[16] S. Li, M. Pomaska, A. Lambertz, W. Duan, K. Bittkau, D. Qiu, et al., Transparent-conductive-oxide-free front contacts for high-efficiency silicon heterojunction solar cells, Joule 5 (2021) 1535–1547.
[17] D.D. Tune, N. Mallik, H. Fornasier, B.S. Flavel, Breakthrough carbon nanotube–silicon heterojunction solar cells, Adv. Energy Mater. 10 (2019).
[18] G. Makrides, B. Zinsser, M. Norton, G. E, Performance of photovoltaics under actual operating conditions, Third Generation Photovoltaics (2012) 201–232.
[19] V. Sharma, A. Kumar, O.S. Sastry, S.S. Chandel, Performance assessment of different solar photovoltaic technologies under similar outdoor conditions, Energy 58 (2013) 511–518.
[20] T. Gageot, F. Jay, J. Veirman, et al., Using thin AZO layers coupled with SiN_x: h as a way to decrease Indium consumption in SHJ cells and modules, Sol. Energy Mater. Sol. Cell. 295 (2026) 113977.
[21] W. Liu, L. Zhang, X. Yang, J. Shi, L. Yan, L. Xu, et al., Damp-Heat-Stable, High-Efficiency, industrial-size silicon heterojunction solar cells, Joule 4 (2020) 913–927.
[22] K. Zhang, O. Mashkov, A. Yaqin Muhammad, et al., Damp-Heat–Induced degradation of lightweight silicon heterojunction solar modules with different transparent conductive oxide layers, Prog. Photovoltaics Res. Appl. 33 (2025) 541–550.
[23] H. Park, J. Jeong, E. Shin, S. Kim, J. Yi, A reliability study of silicon heterojunction photovoltaic modules exposed to damp heat testing, Microelectron. Eng. 216 (2019).
[24] K. Zhang, A. Lambertz, K. Dzięcioł, et al., Towards integrated photovoltaic applications: lightweight silicon heterojunction solar modules with different encapsulation materials and their damp heat stability, Appl. Energy 400 (2025).
[25] J. Hüpkes, J.I. Owen, M. Wimmer, et al., Damp heat stable doped zinc oxide films, Thin Solid Films 555 (2014) 48–52.
[26] D. Greiner, S.E. Gledhill, C. Köble, J. Krammer, R. Klenk, Damp heat stability of Al-doped zinc oxide films on smooth and rough substrates, Thin Solid Films 520 (2011) 1285–1290.
[27] A.B. Morales-Vilches, A. Cruz, S. Pingel, S. Neubert, L. Mazzarella, D. Meza, et al., ITO-Free silicon heterojunction solar cells with ZnO:Al/SiO2 front electrodes reaching a conversion efficiency of 23%, IEEE J. Photovoltaics 9 (2019) 34–39.
[28] D. Adachi, T. Terashita, T. Uto, J.L. Hernández, K. Yamamoto, Effects of SiOx barrier layer prepared by plasma-enhanced chemical vapor deposition on improvement of long-term reliability and production cost for Cu-plated amorphous Si/crystalline Si heterojunction solar cells, Sol. Energy Mater. Sol. Cell. 163 (2017) 204–209.
[29] J. Yu, Y. Bai, Q. Qiu, Z. Sun, L. Ye, C. Qian, et al., Reliability of transparent conductive oxide in ambient acid and implications for silicon solar cells, eScience 4 (2024).
[30] D. Polverini, M. Field, E. Dunlop, W. Zaaiman, Polycrystalline silicon PV modules performance and degradation over 20 years, Prog. Photovoltaics Res. Appl. 21 (2012) 1004–1015.
[31] Q. Tang, W. Duan, A. Lambertz, K. Bittkau, M.A. Yaqin, Y. Zhao, et al., > 85% indium reduction for high-efficiency silicon heterojunction solar cells with aluminum-doped zinc oxide contacts, Sol. Energy Mater. Sol. Cell. 251 (2023).
[32] T. Tohsophon, J. Hüpkes, S. Calnan, W. Reetz, B. Rech, W. Beyer, N. Sirikulrat, Damp heat stability and annealing behavior of aluminum doped zinc oxide films prepared by magnetron sputtering, Thin Solid Films 511–512 (2006) 673–677.

[33] X. Li, Y. Yang, K. Jiang, et al., Potential-free sodium-induced degradation of silicon heterojunction solar cells, Prog. Photovoltaics Res. Appl. 31 (9) (2023) 939–948.
[34] Y. Luo, J. Shi, S. Chen, et al., Sodium-induced degradation of tungsten doped indium oxide film and HJT solar cells in damp-heat environment, Sol. Energy 296 (2025), 113578.5.
[35] X. Wu, C. Sen, H. Wang, et al., Addressing sodium ion-related degradation in SHJ cells by the application of nano-scale barrier layers, Sol. Energy Mater. Sol. Cell. 264 (2024) 112604.
[36] X. Wu, X. Wang, R. Lv, et al., Unveiling the degradation mechanisms in silicon heterojunction solar cells under accelerated damp-heat testing, Sol. Energy Mater. Sol. Cell. 282 (2025) 113325.
[37] W. Duan, A. Lambertz, K. Bittkau, D. Qiu, K. Qiu, U. Rau, K. Ding, A route towards high-efficiency silicon heterojunction solar cells, Prog. Photovoltaics Res. Appl. 30 (2021) 384–392.
[38] Commission IE, IEC 61215-2: Terrestrial Photovoltaic (PV) Modules-Design Qualification and Type Approval-Part 2: Test Procedures, 2021.
[39] O. Breitenstein, Understanding the current-voltage characteristics of industrial crystalline silicon solar cells by considering inhomogeneous current distributions, Opto-Electron. Rev. 21 (2013) 259–282.
[40] P.P. Altermatt, G. Heiser, A.G. Aberle, A. Wang, J. Zhao, S.J. Robinson, et al., Spatially resolved analysis and minimization of resistive losses in high-efficiency Si solar cells, Prog. Photovoltaics Res. Appl. 4 (1996) 399–414.
[41] U. Rau, Superposition and reciprocity in the electroluminescence and photoluminescence of solar cells, IEEE J. Photovoltaics 2 (2012) 169–172.
[42] T. Kirchartz, A. Helbig, W. Reetz, M. Reuter, J.H. Werner, U. Rau, Reciprocity between electroluminescence and quantum efficiency used for the characterization of silicon solar cells, Prog. Photovoltaics Res. Appl. 17 (2009) 394–402.
[43] M. Kasemann, D. Grote, B. Walter, W. Kwapil, T. Trupke, Y. Augarten, et al., Luminescence imaging for the detection of shunts on silicon solar cells, Prog. Photovoltaics Res. Appl. 16 (2008) 297–305.
[44] A.C. Beer, The Hall effect and related phenomena, Solid State Electron. 9 (1966) 339–351.
[45] S. Eriksson, Electronics Letters, Institution of Engineering and Technology IET, 1985.
[46] YSaH. Liu, Chih Yi, Wu, Yen Ju, Wei, Yu Shan, Po Ming Lee, Hsiu Ming Hsieh, Liu, Cheng Yi, Mechanism of conductivity degradation of AZO thin film in high humidity ambient, Appl. Surf. Sci. 282 (2013) 32–37.
[47] J.I. Kim, W. Lee, T. Hwang, J. Kim, S.-Y. Lee, S. Kang, et al., Quantitative analyses of damp-heat-induced degradation in transparent conducting oxides, Sol. Energy Mater. Sol. Cell. 122 (2014) 282–286.
[48] M. Theelen, T. Boumans, F. Stegeman, F. Colberts, A. Illiberi, J. van Berkum, et al., Physical and chemical degradation behavior of sputtered aluminum doped zinc oxide layers for Cu(In,Ga)Se2 solar cells, Thin Solid Films 550 (2014) 530–540.
[49] T.P. Dhakal, M.M. Hamasha, A.S. Nandur, D. Vanhart, P. Vasekar, S. Lu, et al., Moisture-Induced surface corrosion in AZO thin films formed by atomic layer deposition, IEEE Trans. Device Mater. Reliab. 12 (2012) 347–356.